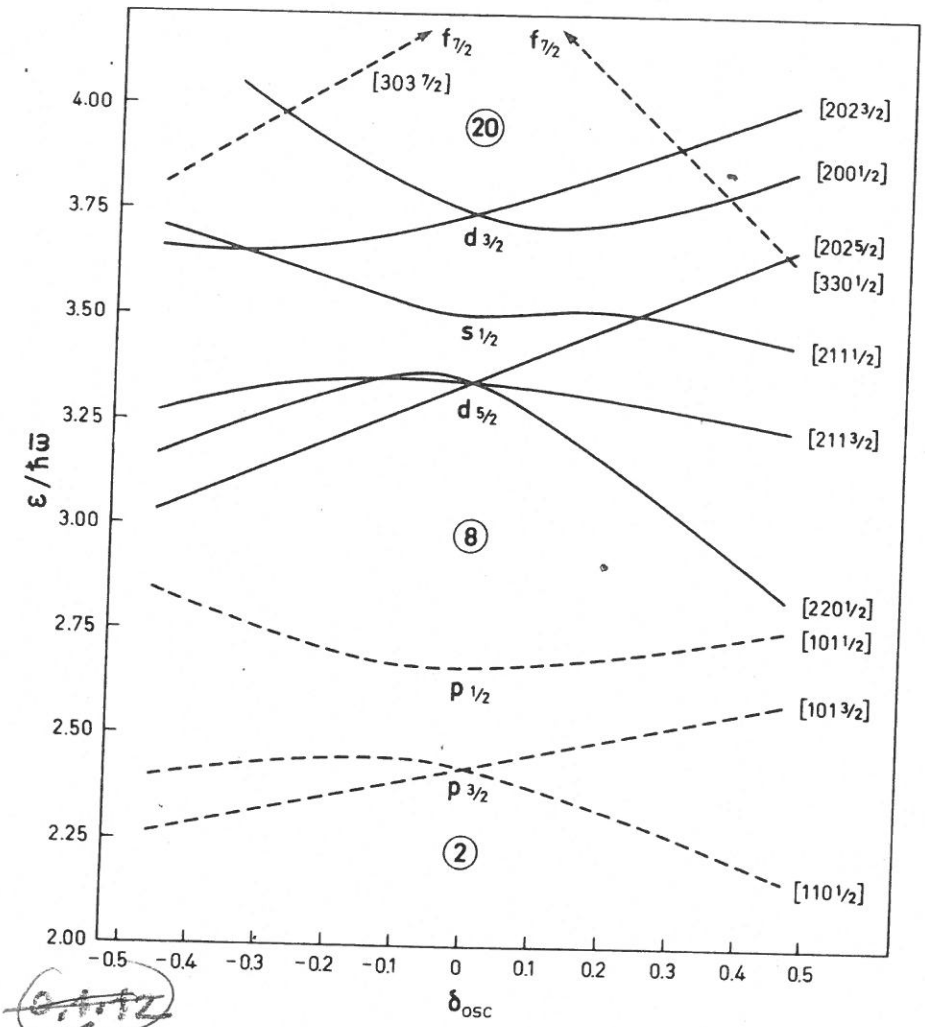

Figure 5-1 Spectrum of single-particle orbits in spheroidal potential (N and $Z < 20$). The spectrum is taken from B. R. Mottelson and S. G. Nilsson, *Mat. Fys. Skr. Dan. Vid. Selsk.* **1**, no. 8 (1959). The orbits are labeled by the asymptotic quantum numbers $[Nn_3\Lambda\Omega]$ referring to large prolate deformations. Levels with even and odd parity are drawn with solid and dashed lines, respectively (after Bohr and Mottelson (1975)).

0.4.2

Bohr and Mottelson Vol II Fig 5-1 + caption

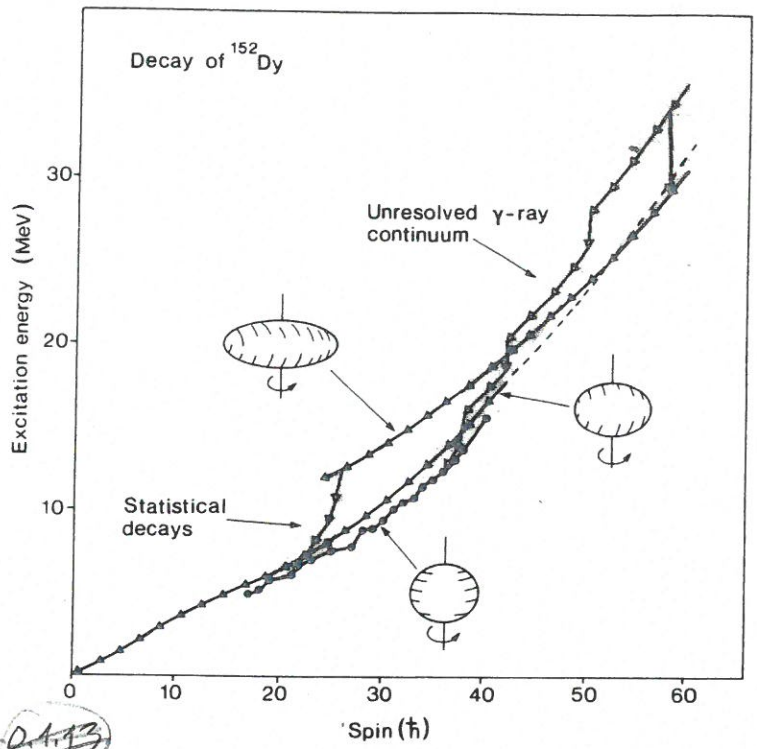

0.4.13

Figure 8 A schematic of the proposed γ-ray decay paths from a high-spin entry point in ^{152}Dy. The major initial decay flow occurs mainly via E2 transitions in the unresolved γ-ray continuum and reaches the oblate yrast structures between 30ħ and 40ħ. A small 1% branch feeds the superdeformed band, which is assumed to become yrast at a spin of 50–55ħ. The deexcitation of the superdeformed band around 26ħ occurs when the band is 3–5 MeV above yrast, and a statistical type of decay flow takes it into the oblate states between 19ħ and 25ħ. The diagram also shows the low deformation prolate band. (After Nolan and Twin (1988)).

P. J. Nolan and P. Twin, Superdeformed shapes at high angular momentum, Ann. Rev. Nucl. and Particle Science, 38, 533 (1988)

0.4.7

Fig 0.4.3

↑ Figura cogida de este articulo

y caption

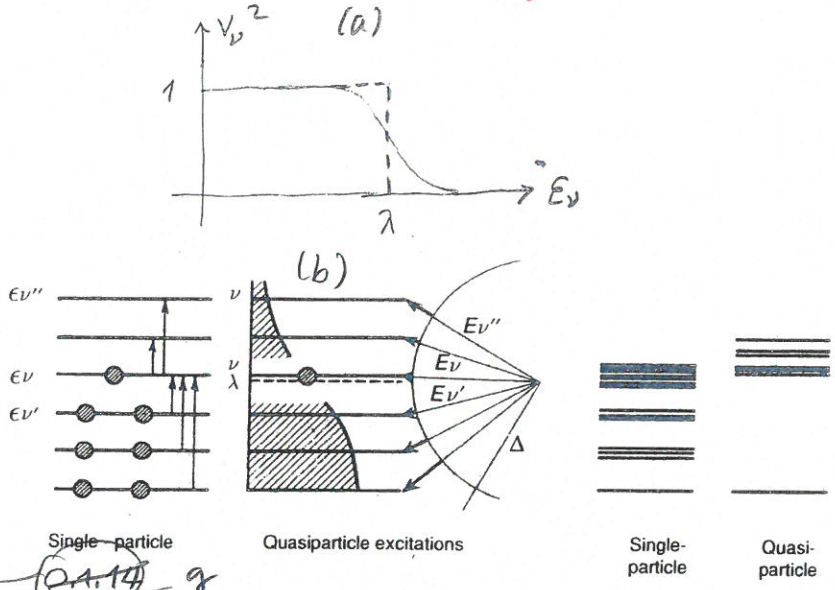

0,4,4

4

0,4,3

0,4,14 g

Figure ~~1.8.~~ Ground state and excited states in the extreme independent single-particle model and in the pairing-correlated, superfluid model in the case of a system with an odd number of particles. In the first case, the energy of the ground state of the odd system differs from that of the even with one particle fewer by the energy difference $\varepsilon_\nu - \varepsilon_{\nu'}$, while in the second case by the energy $E_\nu = \sqrt{(\varepsilon_\nu - \lambda)^2 + \Delta^2} \approx \Delta$, associated with the fact the odd particle has no partner. Excited states can be obtained in the independent particle case by promoting the odd particle to states above the level ε_ν, or by exciting one particle from the state below to the state ε_ν or to one above it. To the left only a selected number of these excitations are shown. In the superfluid case excited states can be obtained by breaking of pairs in any orbit. The associated quasiparticle energy is drawn also here by an arrow of which the thin part indicates the contribution of the pairing gap and the thick part indicates the kinetic energy contribution, i.e. the contribution arising from the single-particle motion. Note the very different density of levels emerging from these two pictures, which are shown at the far left of the figure (after Nathan and Nilsson (1965)). Reprinted from *Alpha- Beta- and Gamma-Ray Spectroscopy*, Vol. 1, Nathan, H. and Nilsson, S. G., Editor Siegbahn, H., page 601, Copyright 1965) ~~with permission from Elsevier.~~

(a) Independent (dashed line) and BCS occupation numbers; (b)

Figura

Use Fig. 4.1 p. 78
Brunk + Broglia

also the same caption

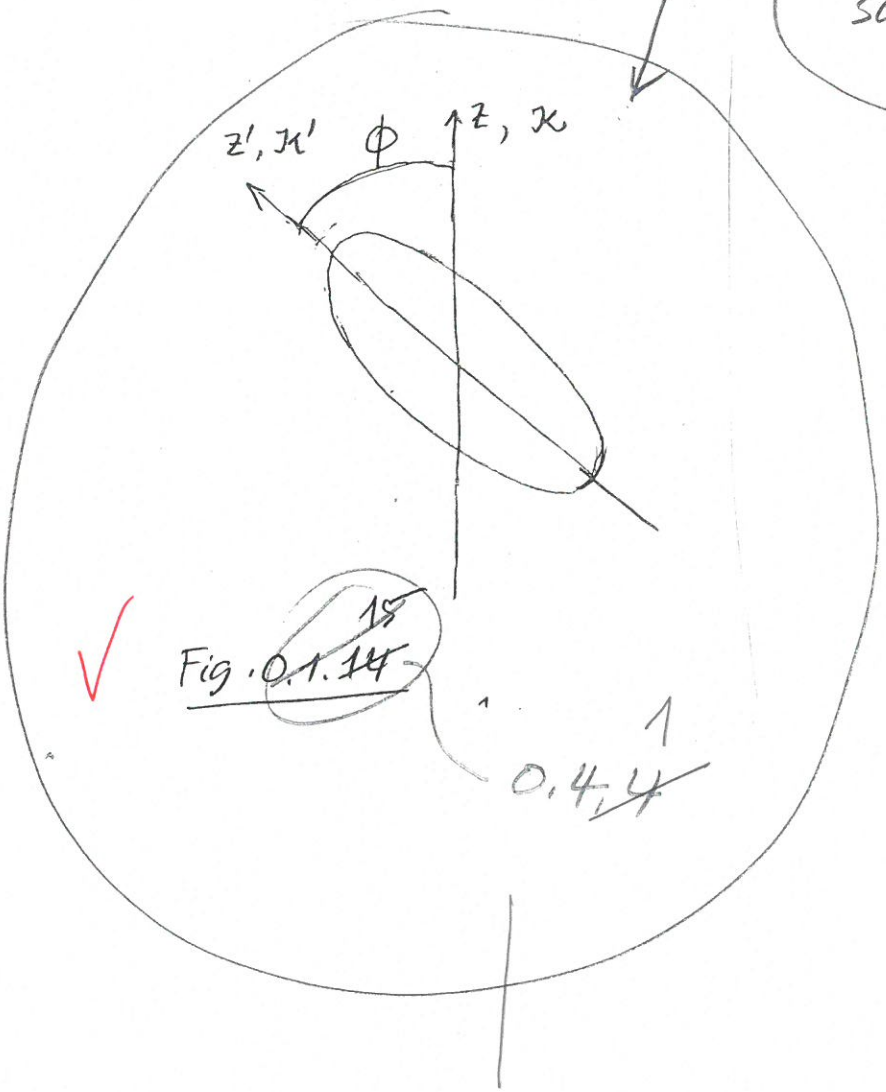

~~15~~
Fig. 0.1.~~14~~

1
0.4.~~4~~

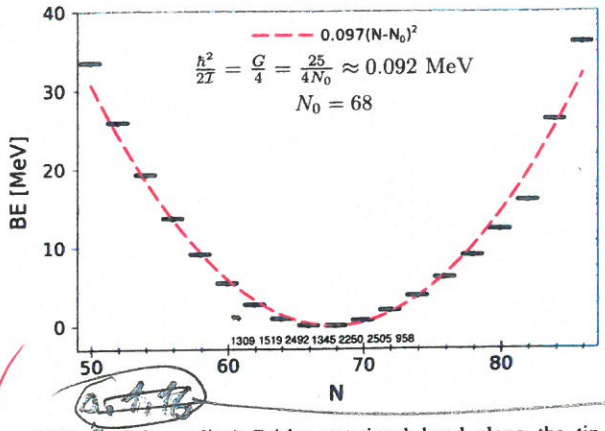

FIG. 9. (Color online) Pairing rotational band along the tin isotopes. The lines represent the energies calculated according to the expression $BE = B(^{50+N}\mathrm{Sn}_N) - 8.124N + 46.33$ [10], subtracting the contribution of the single nucleon addition to the nuclear binding energy obtained by a linear fitting of the binding energies of the whole Sn chain. The estimate of $\hbar^2/2\mathcal{I}$ was obtained using the single j-shell model (see, e.g., Ref. [10], Appendix H). The numbers given on the abscissa are the absolute value of the experimental gs → gs cross section (in units of μb) see Table IV).

0, 4, 5

After Patel et (2013)

Sn-isotopes

Figura y Caption

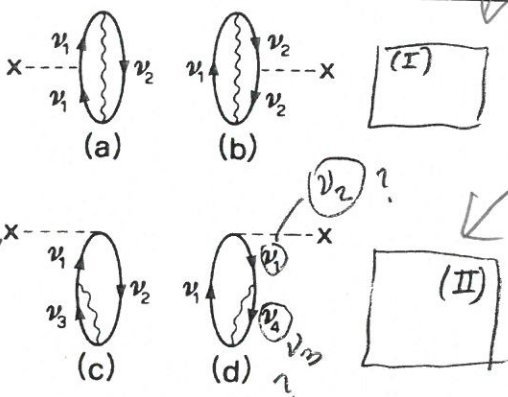

FIG. 1. Lowest-order corrections in the particle-vibration coupling vertex of the nuclear density due to the presence of zero-point fluctuations associated with density vibrations. An arrowed line pointing upwards denotes a particle, while one pointing downward a hole. A wavy line represents a surface phonon. The density operator is described through a dotted horizontal line starting with a cross. Graphs (a) and (b) are typical examples of density contributions to $\delta\rho$, (c) and (d) are of potential contributions.

As expected, fluctuations of the surface remove matter from inside the nucleus and place it on the surface region. The most important contributions arise from low-lying ($T=0$, $I^\pi=3^-,5^-$) collective vibrations. From the point of view of the single-particle motion the associated surface fluctuations display very low frequencies and lead to an ensemble of deformed shapes. Nucleons can thus reach into distances from the nuclear center which are considerably larger than the radius R of the static spherical potential. Because the frequencies of the giant resonances ($T=1$ and $T=0$, $I^\pi=2^+,3^-4^+,5^-$) are of similar magnitude to those corresponding to the single-particle motion, the associated surface deformations are averaged out.

On account of the presence of smaller energy denominators, the single-particle renormalization contributions [cf. graphs (c) and (d) of Fig. 1] are much larger than the vertex-type contributions [graphs 1(a) and 1(b)]. In fact $\simeq$70% of the total effect arises from the first type of diagrams [cf. Table I and Fig. 2(A)]. Similar results were obtained by Khodel, Platanov, and Saperstein.[8]

Because graphs 1(c) and 1(d) contain scattering vertices, to calculate their contribution one has to go beyond the RPA. This is the reason why in Ref. 4, where only RPA process were considered, $\delta\rho$ was found to be very small.

A rather general argument can be made of why a calculation including only graphs 1(a) and 1(b) is not correct. All four graphs 1(a)–1(d) constitute a set of sum-rule conserving graphs fulfilling the Ward identity.[9] In particular, in the case of a monopole vibration the cancellation between all four contributions reflects the conservation of the number of particles (cf. Refs. 10–13). The reason why the cancellation between graphs 1(a) and 1(b) is more complete than between 1(c) and 1(d) is to be found in the fact that while the terms of the type 1(a) correspond to one-to-one with those of type 1(b), many more terms occur of the type 1(c), in which a particle is scattered, than of type 1(d), in which a hole is scattered.

In Fig. 2(B) and Table I we compare the results of the present calculations to those of the macroscopic model of Ref. 5, where the problem of the divergence of the zero-point fluctuations of the liquid drop[14] was solved, and where the role played by surface fluctuations in the static nuclear properties was emphasized.

It can be seen that both methods give rather large and

TABLE I. Contribution to the mean square radius of ^{40}Ca arising from the zero-point fluctuations associated with surface vibrations whose multipolarity is indicated in the first column. In columns marked (a)+(b) and (c)+(d) under the heading Micr., the summed contributions of the corresponding graphs of Fig. 1 are displayed including the coupling of all the phonons of each multipolaritiy (100% energy-weighted sum rule). The separate contributions for isoscalar and isovector vibrations are shown. Under the heading (a)+(b)+(c)+(d) the total summed contribution of the processes shown in Fig. 1 are displayed. The contribution of the low-lying modes to these values are shown in parentheses. Under the heading Macr., the macroscopic results calculated according to Ref. 5 are displayed. The summed contributions for all types of processes are 0.935 (Micr.) and 0.659 (Macr.).

	$\delta\langle r^2\rangle$ (fm^2)							
	$T=0$				$T=1$			
	Micr.			Macr.	Micr.			Macr.
	(a)+(b)	(c)+(d)	(a)+(b)+(c)+(d)		(a)+(b)	(c)+(d)	(a)+(b)+(c)+(d)	
2^+	0.017	0.028	0.045	0.045	0.003	0.005	0.008	−0.014
3^-	0.093	0.384	0.477	0.437	0.008	0.015	0.023	−0.042
			(0.371)					
4^+	0.037	0.054	0.091	0.110	0.010	0.013	0.023	−0.042
5^-	0.065	0.169	0.234	0.240	0.014	0.020	0.034	−0.075
			(0.123)					
Total	0.212	0.635	0.847	0.832	0.035	0.053	0.088	−0.173

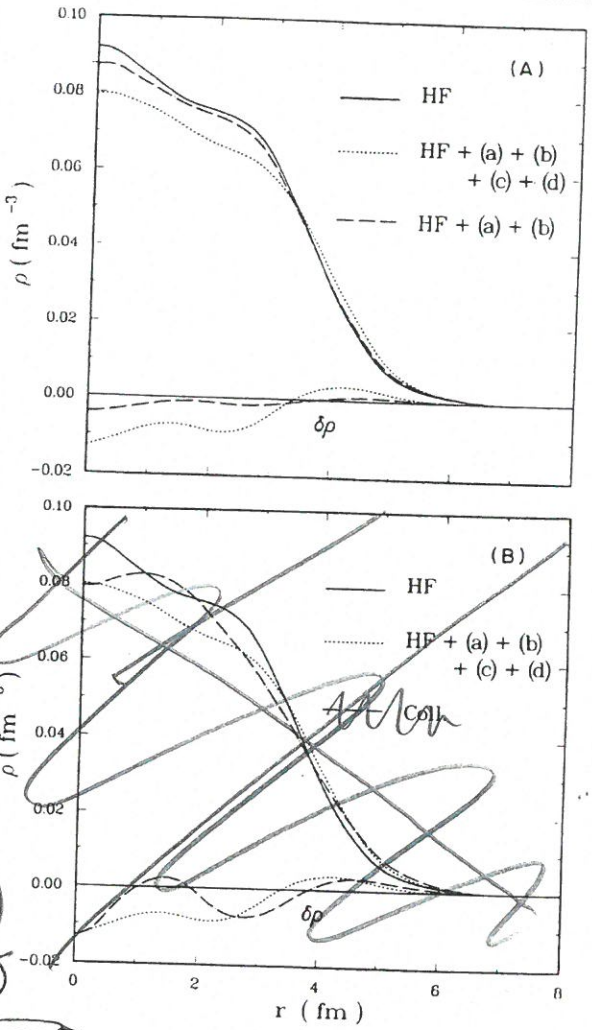

FIG. 2. Modification in the charge density of ^{40}Ca induced by the zero-point fluctuations associated with vibrations of the surface modes. In (A) we show the results of the microscopic calculations presented in this paper. The results labeled HF, HF + (a) + (b), and HF + (a) + (b) + (c) + (d) are the Hartree-Fock density, and that resulting from adding to it the corrections $\delta\rho$ associated with the processes (a) + (b) and (a) + (b) + (c) + (d) displayed in Fig. 1, respectively. In the lower part of the figure the corresponding quantities are displayed. In (B) these results are compared to the macroscopic calculations of Ref. 5.

similar corrections to the mean square radius (cf. the summed contributions at the bottom of Table I). However, the almost perfect agreement between the individual isoscalar contributions of the two models is somewhat misleading. In this connection we point to the negative contributions of the macroscopic model associated with isovector ($T=1$) vibrations. They arise from a (small) term, linear in the strength of the residual interaction which cancels, to a large extent (exactly in the case of interactions with Serber character, cf. Appendix of Ref. 5, with an analogous but positive linear term present in the isoscalar ($T=0$) channel. This is gratifying, as the lowest-order corrections to the fluctuations of the ground state should be quadratic in the residual interaction. Consequently, it is only the summed $[(T=0)+(T=1)]$ contributions which are meaningful in the macroscopic model.

The radial dependence of $\delta\rho$ (cf. Fig. 2) shows maxima and minima out of phase with the Hartree-Fock density displaying, at the nuclear surface, a contribution of the order of 10% of ρ. Fluctuations of the nuclear surface lead to a smoothing of the oscillations of the density and also to an increase in the radius and in the diffusivity of the nucleus. This can be seen in Fig. 2(A), where the microscopic corrections, as well as the Hartree-Fock and the total densities are displayed.

The macroscopic and microscopic results agree well in the surface region [cf. Fig. 2(B)], while the oscillations predicted by the macroscopic model, in the nuclear interior, are more pronounced. In any case, the fact that in the collective approach $\delta\rho \sim \partial^2\rho/dr^2$ (see Broglia[15]) clarifies the phase relation existing between the oscillators in ρ and $\delta\rho$.

The relative change of the mean square radius predicted by the microscopic calculations presented above is $\delta\langle r^2\rangle/(\frac{3}{5}R_0^2) \lesssim 5\%$, in agreement with the results of Ref. 5.

We conclude that the parameters of the effective forces used in Hartree-Fock calculations should not be adjusted to fit the static nuclear properties, but only after the zero-point fluctuations of the surface have been taken into account.

One of us (F.B.) wants to acknowledge economic support from the Spanish Comisión Asesora de Investigación Cientifica y Técnica. Discussions with G. F. Bertsch and H. Esbensen are gratefully acknowledge.

---

[a]Present address: Escuela Superior de Ingenieros Industriales, Avda. Reina Mercedes, Sevilla, Spain.

[1]A. Bohr and B. R. Mottelson, *Nuclear Structure* (Benjamin, Reading MA, 1975), Vol. 2.

[2]P. F. Bortignon, R. A. Broglia, D. R. Bes, and R. Liotta, Phys. Rep. **30C**, 305 (1977).

[3]G. F. Bertsch and S. F. Tsai, Phys. Rep. **18C**, 125 (1975).

[4]D. Gogny, in *Nuclear Physics with Electromagnetic Interactions*, edited by H. Arenhövel and D. Drechsel, Lecture Notes in Physics, Vol. 108 (Springer-Verlag, New York, 1979), p. 88.

[5]H. Esbensen and G. F. Bertsch, Phys. Rev. C **28**, 355 (1983).

[6]P. G. Reinhard and D. Drechsel, Z. Phys. A **290**, 85 (1979).